Mapping densely packed GPIIb/IIIa receptors in murine blood platelets with expansion microscopy

Hannah S. Heil[1], Max Aigner[1], Sophia Maier[1], Prateek Gupta[1], Luise M.C. Evers[1], Vanessa Göb[1,2], Charly Kusch[1,2], Mara Meub[3], Bernhard Nieswandt[1,2], David Stegner[1,2*] and Katrin G. Heinze[1*]

[1] Rudolf Virchow Center for Integrative and Translational Bioimaging, University of Würzburg, Würzburg, Germany

[2] Institute of Experimental Biomedicine I, University Hospital Würzburg, Würzburg, Germany

[3] Department of Biotechnology and Biophysics, Biozentrum, University of Würzburg, Würzburg, Germany

* corresponding authors:

Katrin G. Heinze (katrin.heinze@virchow.uni-wuerzburg.de)

[1]Rudolf Virchow Center for Integrative and Translational Bioimaging, University of Würzburg, Würzburg, Germany

or David Stegner (stegner@virchow.uni-wuerzburg.de)

[2]Institute of Experimental Biomedicine, University Hospital Würzburg, Würzburg, Germany
`

Running title: Mapping platelet receptors with ExM

1 **Abstract**

2 Interrogating small platelets and their densely packed, highly abundant receptor
3 landscape is key to understand platelet clotting, a process that can save lives when
4 stopping blood loss after an injury, but also kill when causing heart attack, stroke or
5 pulmonary embolism. The underlying key receptor distributions and interactions, in
6 particular the relevance of integrin clustering, are not fully understood is because of highly
7 abundant and densely distributed GPIIb/IIIa receptors. This makes receptor distributions
8 difficult to assess even by super-resolution fluorescence microscopy. Here, we combine
9 dual-color expansion and confocal microscopy with colocalization analysis to assess
10 platelet receptor organization without the need of a super-resolution microscope. We show
11 that 4x expansion is highly straight-forward for super-resolution microscopy of platelets,
12 while 10x expansion provides higher precision at the price of increased efforts in sample
13 preparation and imaging. Quantifying various receptor colocalization scenarios we
14 demonstrate that expansion microscopy can pinpoint receptor distributions and
15 interactions in resting and activated platelets being superior to conventional methods that
16 fail in such dense 3D scenarios with highly abundant receptors. We reveal the presence
17 of GPIIb/IIIa clusters in resting platelets, which are not affected by platelet activation
18 indicating that they contribute to the rapid platelet response during platelet clotting.

19 **Graphical Abstract**
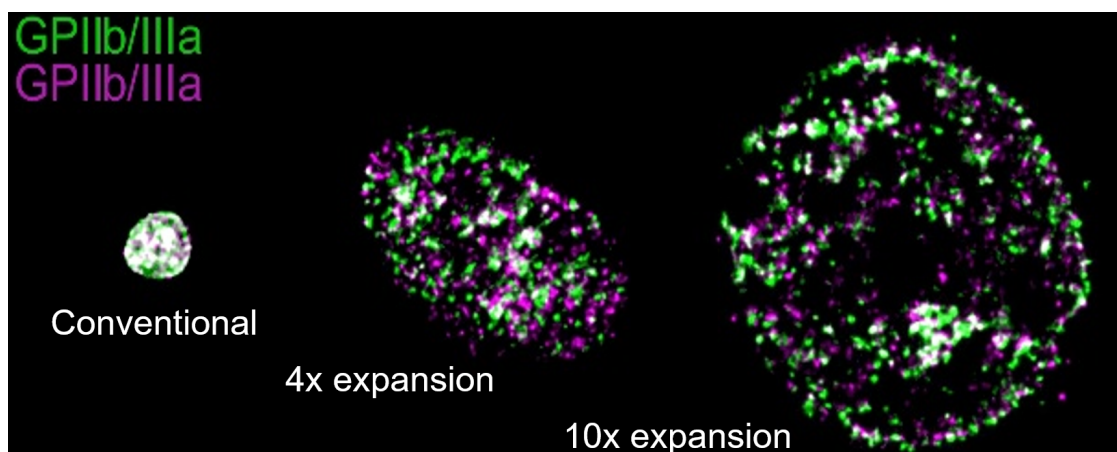
20 **Keywords:** Integrin, blood platelets, receptor mapping, super-resolution microscopy,
21 colocalization

Introduction

23   Integrins are a superfamily of heterodimeric cell-surface receptors that comprise an α and

24   a β subunit.[1,2] Each subunit consist of a large N-terminal extracellular domain that

25   contributes to ligand binding, a single-pass transmembrane domain and a cytoplasmic tail

26   providing binding sites for adaptors, and signaling proteins that contribute to the

27   bidirectional integrin signaling.[3,4] Integrin receptors are widely expressed in mammalian

28   tissues and serve as adhesive units, which are, however, highly dynamic regulators of

29   cellular responses. This is in particular true for platelets that require an acute and dynamic

30   regulation of integrin affinity and ligand binding to enable rapid platelet adhesion at sites

31   of vascular injury on the one hand and to prevent uncontrolled thrombosis of the other

32   hand. The αIIbβ3 integrin (also named GPIIb/IIIa or CD41/CD61) is exclusively expressed

33   by megakaryocytes and platelets and binds a number of ligands, including fibrinogen,

34   fibrin, fibronectin and von Willebrand factor.[5] This receptor is of high clinical relevance as

35   GPIIb/IIIa inhibitors are widely used to prevent thrombosis and treat myocardial infarction.[6]

36   Moreover, GPIIb/IIIa serves as model receptor to study integrin biology.[4] In the last

37   decades key components of both inside-out and outside-in signaling have been identified;

38   the first represents the functional up-regulation of the receptor's affinity, the latter

39   generates integrin-mediated signaling responses following ligand binding.[3,4] In addition, it

40   is widely accepted that clustering of integrin receptors in hetero-oligomers modulates

41   avidity and supports the assembly of the outside-in signalosome;[7,8] unfortunately, our

42   current understanding of the underlying processes and the receptor distribution is far from

43   complete.[4,9] One reason is the high receptor density on the platelet surface. Platelets are

44   small in size (2-3 μm in diameter) and express 50,000-100,000 copies of GPIIb/IIIa on

45   their surface, while even more can be mobilized from intracellular stores.[10,11] Thus,

46   visualizing and quantifying GPIIb/IIIa distribution on the platelet surface is very

47   challenging. Strictly spoken, a resolution in the nanometer range is required to gain an

48   image based receptor map on the single molecule level.[12] Electron microscopy would

49   provide such nanometer resolution, however, despite its unrivaled resolution power, it

50   lacks efficient staining for specific receptors and immunogold labeling is hard to achieve

51   at saturating conditions. In contrast, fluorescence labeling is efficient and selective and

52   thus allows visualization of single membrane receptors when combined with super-

53   resolution imaging.[13–15] A variety of fluorescence super-resolution modalities have been

54   reported over the past century, each with its own advantages and limitations.[16] Multi-color

55   3D single molecule localization microscopy allows to effectively decipher receptor

56   interaction and organization at a molecular level; however, it requires a high level of

57   expertise and equipment and fails at high molecular density scenarios[17] such as highly

58   abundant and dense platelet receptor distributions we are tackling here. A particularly

59   promising, rather young method is expansion microscopy (ExM).[18] In contrast to most

60   other super-resolution techniques ExM does not require a high-end super-resolution

61   microscope but uses physical volumetric expansion of the sample. Linking the

62   fluorescently labeled proteins to a swell-able hydrogel eventually turns any conventional

63   microscope into a super-resolution imaging device. The major downside is that isotropic

64   expansion requires a highly processed sample and harsh preparation steps: After fixation

65   and immunolabeling the sample structure itself needs to be tightly linked into the hydrogel

66   network and has to be disrupted by breaking protein bonds and crosslinks through either

67   protein digestion or degradation[19]. Depending on the hydrogel composition the gel will

68   swell up to 10x of its original size expanding the sample to up to 1000x of its original

69   volume[20] (see also supplemental Figure I). With physical expansion, the labeling density

70   decreases respectively, and the sample additionally undergoes harsh chemical treatment

71   during gelation and digestion, which typically results in a 50% loss of fluorescent

72   markers.[19] Nevertheless, the resolution gain by ExM allows quantitative image-based

73   comparison of two (fluorescently labeled) molecular distributions. Eventually, a

74   colocalization coefficient can be calculated providing an intensity correlation measure of

75   both color channels.[21] The commonly used Pearson's colocalization coefficient excels in

76   robustness under varying signal-to-noise conditions, however fails when number of events

77   detected in each channel are not comparable. The two Manders' colocalization

78   coefficients are less robust to noise, but make analysis more versatile as the approach

79   allows to directly retrieve the overlapping fraction of one protein to the other and vice

80   versa.[22] In ExM reporting the overlapping fraction regardless of the degree of asymmetric

81   signal loss in both channels is crucial.

82   Here we show how ExM and image analysis can be tuned to advance studies of dense

83   and highly abundant platelet receptor interactions, which are difficult to tackle otherwise.

84   Our quantitative approach involves a combination of ExM, confocal microscopy and

85   colocalization analysis with optimized sample preparation for 4x and 10x expansion as

86   well as tailored image analysis pipelines. Supported by a simulation tool for platelet

87   receptor distributions we find that only 10x expansion provides the required resolution to

88   distinguish colocalized from independent receptor distributions for highly abundant

89   GPIIb/IIIa and GPIX receptors on resting and activated platelets.

Methods

91   The authors declare that materials and data are available upon reasonable request from

92   the authors. A selection of typical images and the code for simulation of platelet receptor

93   distributions are available on ZENODO (doi: 10.5281/zenodo.4117555), where we also

94   provide a video protocol of the sample preparation for 10x ExM. An extended version of

95   Materials and Methods as well as detailed supplementary protocols for 4x and 10x platelet

96   ExM are available in the Supplemental Material. All methods were carried out in

97   accordance with relevant guidelines and regulations.

Platelet Isolation

99   C57Bl/6J mice served as blood donors and animal experiments were approved by the

100   district government of Lower Franconia (Bezirksregierung Unterfranken). Washed

101   platelets were prepared as described elsewhere[23]. Round coverslips (Ø12 mm, #1.5 , #1.5

102   Menzel and Ø24 mm, #1.5 Plano GmbH) were cleaned by 1 h sonication in chloroform

103   (472476, Sigma), followed by 1 h sonication in NaOH (6771, Roth), ddH$_2$O washed, dried

104   at 70°C and stored in Ethanol (34852, Sigma). The clean coverslips were coated with 2 M

105   glycine (A1067, AppliChem) in PBS for 10 min and washed 2x with PBS and 1x with

106   Tyrodes buffer. The platelet suspension was deposited onto the coated coverslips ($30*10^6$

107   / $15*10^6$ platelets for 24 mm/12 mm) and incubated for 30 min at 37°C for settling. Platelet

108   activation was achieved by complementing the Tyrodes buffer with 2 mM Ca^{2+} and the

109   addition of 0.01 U/ml Thrombin (10602400001, Roche) to the platelet suspension.

Immunostaining

111   *Fixation:* Platelets were fixed with glyoxal solution (19.89% (wt/wt) pure ethanol, 3.15%

112   (wt/wt) glyoxal (128465, Sigma), 0.7% (wt/wt) acetic acid (7332.1, Roth) in ddH$_2$O) at pH

113   5.0 for 20 min [24] at RT, washed 5x with PBS and blocked with 5% bovine serum albumin

114   (BSA, A3983, Sigma) in PBS for 2 h, then washed with PBS.

115   *Immunolabeling*: Platelets were immersed in 10 µg/ml fluorescently labeled antibody

116   (produced in-house: IgG MWReg30 against GPIIb/IIIa, IgG JON6 against GPIIb/IIIa on

117   different epitope, and IgG p0p6 against GPIX as described previously[25]) conjugated with

118   Alexa Fluor 488 (A20181, Thermo Fisher) or Alexa Fluor 594 (A20185, Thermo Fisher)

119   solved in PBS with 5% BSA for 30 min at 37°C, ensuring saturated labeling of all available

120   epitopes (tested with flow cytometry). Afterwards, coverslips were washed 5x with PBS.

121   The antibodies' degree of labelling was measured by spectrometric analysis (NanoDrop

122   One, Thermo Fisher Scientific).

Platelet Expansion

124   *4x expansion* (adapted from Chozinski et al 2016 [26]). Immunolabeled platelets on

125   coverslips were incubated at RT with linking solution (0.1 mg/ml Acryloyl-X in PBS,

126   A20770, Invitrogen) for 12 h. A 50 µl drop of monomer solution (2 M NaCl, 2.5% (wt/wt)

127   acrylamide (AA, A9099, Sigma), 0.15% (wt/wt) N,N′-methylenebisacrylamide (M7279,

128   Sigma), 8.625% (wt/wt) sodium acrylate (SA, 408220, Sigma) in PBS), containing 0.2%

129   freshly added ammonium persulfate (APS, 9592.3, Roth) and tetramethylethylenediamine

130   (TEMED, 2367.3, Roth) was placed on elastic film (parafilm, Sigma) and covered by the

131   sample glass coverslip (2x washed with PBS). After gelation for 2 h at RT in a humidified

132   chamber the samples were transferred into digestion buffer (8 U/ml Proteinase K (P4850,

133   Sigma), 50 mM Tris pH 8.0, 1 mM EDTA (ED2P, Sigma), 0.5% Triton X-100 (28314,

134   Thermo Fisher) and 0.8 M guanidine HCl (50933, Sigma) in ddH$_2$O), and incubated

135   overnight (8 h) in a humidified chamber. After removal of the coverslip the gel was

136   expanded in ddH$_2$O for 24 hours, immobilized on a poly-D-lysine (02102694, MP

137   Biomedicals) coated Ø24 mm, #1.5 coverslip and imaged.

138   *10x expansion* (adapted from Truckenbrodt *et al*. 2018 [27] and modified). The 10x monomer

139   solution consists of 2.67% (wt/wt) N,N-dimethylacrylamide (DMAA, 274135, Sigma), and

140   0.64% (wt/wt) sodium acrylate (SA) in ddH$_2$O and was bubbled with N$_2$ to purge out

141   molecular oxygen for 40 min on ice before adding 0.0036 g/ml of KPS (206224, Sigma).

142   After another 15 min of O$_2$ purging 0.4% TEMED were added, and 50 µl of final monomer

143   solution immediately placed on elastic film and covered with the sample (on coverslip).

144   After gelation in a N$_2$-filled humidified chamber for 48 h at 4°C, digestion was performed

145   for 12 h at 50°C.

Fluorescence Imaging

147   Dual color confocal microscopy was used (Leica TCS SP5 II; 63x 1.2 NA water immersion

148   objective, 8000 Hz resonant scanning; pixels: 1024x1024, voxels: x,y = 41 nm & z=170

149   nm, pinhole: 1 Airy unit, scanning: 8x line averaging, 3 frames accumulated, exc.: 488 nm

150   & 561 nm, detection: 500-550 and 600-650 nm in sequential mode, Hybrid detector (HyD).

151   Chromatic aberrations were corrected by distortion matrices using bUnwarpJ[28] (calibration

152   by 100 nm 4-colour fluorescent microspheres (TetraSpeck, T7279) as described

153   elsewhere[29]). Images were deconvolved (Huygens Professional, SVI, Leiden,

154   Netherlands) with a theoretical PSF and a signal-to-noise threshold of 30 counts.

155   **Data Analysis**

156   Image preprocessing, colocalization analysis and statistical validation, as well as the

157   simulation, dSTORM imaging and analysis are described in detail in the *Online*

158   *Supplementary Methods*.

159

160   **Results**

161   **Optimizing ExM for receptor colocalization on platelets**

162   The accuracy of a colocalization study mainly depends on the spatial resolution of the

163   underlying image.[12] In order to compare the performance of the colocalization analysis for

164   different resolution levels, we established two different kinds of expansion protocols

165   leading to 4x and 10x expansion along previously published work.[19,27] Before

166   immunolabeling and expansion, purified resting platelets are settled on a glycine coated

167   surface and chemically fixed without any signal compromise (supplemental Figure II A,B)

168   to avoid unintended receptor reorganization by platelet activation. Here, glyoxal fixation

169   outperformed PFA fixation in both, labeling efficiency and minimal background signal[24]

170   (supplemental Figure II C,D).

171   Figure 1A shows the respective deconvolved confocal images of GPIIb/IIIa receptors on

172   unexpanded versus 4x and 10x expanded platelets. The GPIIb/IIIa receptors are targeted

173   by monoclonal antibodies carrying *either* an Alexa Fluor 594 (Figure 1, magenta) *or* an

174   Alexa Fluor 488 marker (Figure 1, green). Thus, this assay is designed to show low

175   colocalization if resolution is sufficient and clustering is low. For unexpanded small

176   platelets, however, low image resolution leads to a linear relationship in the intensity

177   scatter plot for the two color channels (Figure 1B). Such largely overlapping color signals

178   only provide a meaningless high degree of – potentially false-positive – co-localization. In

179   contrast, with 4x and 10x expanded platelets this linear relationship vanishes and

180   colocalization analysis becomes discernible for different scenarios (Figure 1 C, D).

181   Unfortunately, the resolution gain is accompanied by a loss in contrast due to reduced

182   signal-to-noise ratio (Figure 1E). Moreover, the signal retention varies for different

183   fluorescent dyes. While both antibodies were decorated with a similar number of

184   fluorophores (see supplemental Table I), the signal retention is different for each color

185   (Figure 1F, lower signal retention in the green channel than in the magenta channel). Low

186   contrast and different degree of receptor visibility between channels require a careful

187   preselection of the colocalization modality.

188   The Manders' colocalization approach turned out to be the only applicable here as it is

189   most crucial that the channel with fewer events still reports its overlapping fraction

190   regardless of the degree of asymmetric signal loss in both channels. As the Manders'

191   colocalization coefficient, however, is less robust against noise than the commonly used

192   Pearson's colocalization coefficient, image preprocessing is required to exclude

193   background signal efficiently.[13] Along these requirements, we compiled an image

194   processing pipeline providing a chromatic shift correction (Figure 2A) before a

195   deconvolution step (Figure 2B) followed by background filtering (Figure 2 C,D). In the last

196   step signal events are filtered by intensity threshold and size (detailed description in the

197   supplementary methods).

198   **Receptor distributions revealed by expansion of platelets**

199   ExM increases the optical resolution level to the nanometer range; the exact resolution

200   gain depends on the hydrogel composition and the respective expansion factor. This

201   means that in principle a lateral resolution of down to 25 nm can be realized by 10x

202   expansion and confocal microscopy; however, as this resolution gain comes at the

203   expense of image brightness and contrast, we carefully dissected the resolution level that

204   is required for colocalization analysis of the platelet receptors. First, we used realistic

205   simulations (see Figure 3 and 4) to understand how the image quality and specificity would

206   manifest itself under real experimental conditions. Therefore, randomly distributed single

207   GPIIb/IIIa receptors or receptor clusters as fluorescent objects were computationally

208   placed on a spheroid surface reflecting typical mouse platelet dimensions (Figure 3). From

209   such platelet-like objects (Figure 3A) fluorescence images (Figure 3B-D representing

210   maximal (left) and minimal (right) colocalization) were created including realistic

211   background signal and noise (unexpanded: Figure 3B, 4x expanded: Figure 3C, 10x

212   expanded: Figure 3D). The resulting signal-to-noise ratios of these simulated 3D images

213   for all three expansion levels (none, 4x, 10x) and the two colocalization cases in

214   comparison are plotted in dependence of increasing marker retention ratio. Even if the

215   signal-to-noise level is higher for lower expansion factors, the colocalization coefficient

216   becomes meaningless when looking at platelet receptor distributions with varying

217   densities (Figure 4A) for a high and low colocalization test case (Figure 4B). For the high

218   colocalization case, two markers can bind to one individual receptor at the same time

219   giving rise to a high colocalization coefficient, while in the low colocalization case the two

220   markers have less chance to colocalize as each receptor can only by occupied by either

221   one marker (Figure 4B). In unexpanded platelets it is impossible to distinguish both cases

222   reliably while this was possible for expanded platelets in the whole receptor density range.

223   For a receptor density in the range ~500 /μm^2 as we found for GPIIb/IIIa (see supplemental

224   Figure III) 4x expansion is expected to only show a 10% drop in colocalization between

225   the high and low case, while at 10x expansion a drop of 50% can be expected (Figure

226   4A). Thus, only 10x expansion provides sufficient dynamic range to pinpoint the

227   differences of receptor colocalization in the two test cases. This advantage vanishes only

228   if marker retention would drop below 50% (Figure 4C). Note that for both, 4x and 10x

229   expansion, the achieved super-resolution is just not sufficient to resolve single molecules

230   and thus may still leave a certain risk to detect "false-positive" colocalizations. Here in this

231   case, even for very low receptor densities a Manders' colocalization coefficient of 0.6 or

232   0.2, respectively, represents the low colocalization case. To understand how the loss of

233   markers during homogenization and expansion influence these results, we additionally

234   accounted for the clustered arrangement of GPIIb/IIIa on resting platelets as observed by

235   single molecule localization microscopy (Figure 4D & supplemental Figure III). Decreasing

236   marker retention in both channels means smaller colocalization values (Figure 4E),

237   particularly in 4x expansion where the dynamic range between high and low colocalization

238   is decreased for retention ratios below 50%; in contrast, for 10x expansion the

239   performance is best maintained even beyond 50%. However, with further decreasing

240   (asymmetric) retention ratio the analysis becomes prone to artifacts (Figure 3 &

241   Figure 4F): When the retention ratio is fixed at 60% in channel A and the retention ratio of

242   channel B ranges from 100% to 20% the results seem to be robust down to only 40%

243   retention in channel B for both 4x and 10x expansion. In 4x expansion the dynamic range

244   between the high and low colocalization are indistinguishable (high and low, Figure 4B) at

245   20% retention in channel B. The high colocalization is experimentally realized with two

246   antibodies carrying either dye molecule or targeting different epitopes on GPIIb/IIIa. Thus,

247   they can bind to a single receptor at the same time (supplemental Figure IV*, case I).*

248   Next, we would like to look at true experimental data. For image preprocessing and

249   analysis, it is important to include only platelets above the largest cutoff and with suitable

250   orientations to avoid bias in the subsequent colocalization analysis (Figure 5). Thus, we

251   excluded not fully expanded platelets from further analysis (Figure 5A), and made sure

252   that subpopulations of platelets with different orientations are correctly reflected in the

253   distribution of Manders' colocalization coefficients (Figure 5 B,C). Now, we are fully

254   prepared to interrogate three different colocalization scenarios: For the high colocalization

255   case two antibodies targeting two different epitopes of GPIIb/IIIa are used carrying Alexa

256   Fluor 488 and Alexa Fluor 594 respectively (Figure 6, case I). For the low colocalization,

257   only one antibody targeting a single epitope of GPIIb/IIIa is used, carrying either Alexa

258   Fluor 488 or Alexa Fluor 594 (Figure 6A, case II). As an additional case (case III, Figure

259   6) we introduce two independent receptors, GPIIb/IIIa and GPIX, which are targeted with

260   distinct fluorophores and no colocalization is expected.

261   For unexpanded platelets (Figure 6A left) high Manders' colocalization coefficients are

262   observed for all three test cases and differences in the marker arrangement are not

263   resolved (Figure 6B). In line with previous reports by others[30] our results here underscore

264   that conventional confocal microscopy completely fails when it comes colocalization

265   studies of densely packed targets. By expanding the platelets 4x the coefficient for case I

266   drops down to ~0.6 due to the limited retention ratio. It can already be distinguished from

267   case III with a dynamic range of 0.15 between maximum and minimum colocalization while

268   the resolution is insufficient to distinguish it from case II. The increase in resolution

269   achieved with 10x expansion allows to extend the dynamic range of the Manders'

270   colocalization coefficient to 0.25. While in the 4x expansion experiments the limited

271   resolution still leads to an apparent Manders' colocalization coefficient of ~0.5 for case II

272   and III, it drops down to ~30% for 10x expansion with a clear separation between the high

273   and low colocalization. Simulated data shows 4x expansion does not provide the

274   resolution required at the given receptor densities. Interestingly, case II yields a higher,

275   but not significantly different colocalization coefficient than case III, maybe due to the

276   higher abundance of the GPIIb/IIIa receptors. Fortunately, a neighbor-distance analysis of

277   10x expanded platelets allows to distinguish colocalized, clustered and non-interacting

278   receptor distributions (supplemental Figure V) overcoming its lack of molecular resolution.

279   In an independent experiment we compared the GPIIb/IIIa distribution on resting and

280   activated platelets to assess whether platelet activation affects the formation of integrin

281   clusters. Surprisingly, GPIIb/IIIa colocalization coefficients of activated platelets were

282   comparable to those in resting platelets (Figure 6C,D), suggesting that the organization of

283   GPIIb/IIIa receptors is conserved during platelet activation.

284

Discussion

286   This study shows that the combination of ExM and confocal imaging is a powerful tool to

287   study platelet receptor organization and interaction in small blood platelets and dense and

288   highly abundant receptor scenarios where other high- and super-resolution methods fail.

289   Conventional confocal microscopy alone is not suited as demonstrated here. Based on an

290   optimized sample preparation and tailored image preprocessing and analysis procedure

291   we developed a colocalization analysis approach which allows to classify the distribution

292   and interaction of high-density platelet receptor populations. Our findings suggest, that

293   GPIIb/IIIa receptors are present in pre-formed clusters already on resting blood platelets.

294   These pre-formed clusters might play a role in enhancing platelet adhesion and

295   aggregation following inside-out activation and thereby contribute to the rapid platelet

296   responses upon vascular injury. The unexpected observation that these clusters are not

297   affected by platelet activation (Figure 6D) supports this hypothesis. These data indicate

298   that – at least in the absence of an immobilized ligand – no significant rearrangement of

299   GPIIb/IIIa clusters relative to each other is observed. One might speculate that these

300   uniformly distributed clusters represent preassembled outside-in signalosomes that are

301   'ready to go' upon integrin-ligand binding or inside-out signaling. Thereby, they enable

302   ligand binding on the entire platelet surface, allowing a rapid response to external stimuli.

303   Clearly, further studies are needed to elucidate the receptor interplay on the platelet

304   surface. In particular, the effects of immobilized ligands on the distribution of GPIIb/IIIa

305   clusters are worth studying, to investigate whether such ligands would result in bigger

306   GPIIb/IIIa clusters along the ligands similar to GPVI.[31,32]On the other hand it is also

307   possible that these uniformly GPIIb/IIIa clusters are critical for the mechanosensing

308   capacity of platelets and potentially platelet migration.[33,34]

309   In any case our study successfully addresses the special requirements posed by the small

310   platelet size and high receptor density. While alternative super-resolution microscopy

311   techniques can provide single molecule resolution, which is not achieved here, the

312   presented approach stands out by its accessibility as it does not require an advanced

313   super-resolution setup. Furthermore, the combination with confocal microscopy allows for

314   the implementation of both, 3D and multicolor imaging, still bottlenecks for many super-

315   resolution techniques.

316   However, regarding colocalization analysis the approach itself holds intrinsic challenges

317   as it not only lacks the mentioned single molecule sensitivity, but also suffers from a

318   significant loss of fluorescent markers. We evaluated the performance of ExM based

319   colocalization analysis regarding receptor density and retention ratios based on simulated

320   GPIIb/IIIa receptor distributions. While an expansion of 4x still provides robust results at

321   retention ratios below 50%, the dynamic range between high and low colocalization is

322   significantly lower than for 10x expansion and especially for receptor densities above

323   1000/µm² only 10x expansion provides sufficient resolution to distinguish both cases. As

324   mentioned before, the marker retention ratio greatly depends on the sample processing

325   as well as the molecular properties of the fluorescent dye. For the organic dyes Alexa

326   Fluor 488 and Alexa Fluor 594 used in this study, retention ratios of ~50% have been

327   reported.[19]

328   The higher resolution achieved by 10x expansion comes at the cost of signal dilution, a

329   longer and harsher sample preparation and a decreased mechanical stability of the

330   hydrogel. To address the issue of signal loss and dilution, several modifications of the

331   anchoring chemistry and homogenization procedure have been reported to allow post

332   expansion labeling.[35–37]

333   Despite these limitations ExM will help to improve our understanding of platelet receptor

334   distribution. This will have implications on our understanding of platelet integrin receptor

335   stoichiometry and spatial organization like in the present study. We have established ExM

336   for murine platelets as this allows to combine this attractive technology with transgenic

337   models to investigate further research questions in the platelet field, like the

338   existence/relevance of clusters of (hem)ITAM receptors,[38,39] lipid rafts[40] or the question

339   whether different pools of α-granules exist in platelets.[41,42] By combining ExM with

340   advanced imaging techniques it is even possible to achieve molecular resolution[37,43–45] if

341   the marker and labeling concept allows. Thus, we believe that ExM for platelet imaging

342   has a bright future and may soon help to decipher complex receptor interactions within the

343   nanometer range.

344

362

369

Disclosures

DS is on the editorial board of *Platelets*. All other authors have no conflicts of interest.

References

1. Hynes, R. O. Integrins: Bidirectional, Allosteric Signaling Machines. *Cell* **110**, 673–687 (2002).

2. Campbell, I. D. & Humphries, M. J. Integrin Structure, Activation, and Interactions. *Cold Spring Harb. Perspect. Biol.* **3**, a004994–a004994 (2011).

3. Shattil, S. J., Kim, C. & Ginsberg, M. H. The final steps of integrin activation: the end game. *Nat. Rev. Mol. Cell Biol.* **11**, 288–300 (2010).

4. Durrant, T. N., van den Bosch, M. T. & Hers, I. Integrin αIIbβ3 outside-in signaling. *Blood* **130**, 1607–1619 (2017).

5. Humphries, J. D. Integrin ligands at a glance. *J. Cell Sci.* **119**, 3901–3903 (2006).

6. Mackman, N., Bergmeier, W., Stouffer, G. A. & Weitz, J. I. Therapeutic strategies for thrombosis: new targets and approaches. *Nat. Rev. Drug Discov.* **19**, 333–352 (2020).

7. Fong, K. P. *et al.* Directly Activating the Integrin αIIbβ3 Initiates Outside-In Signaling by Causing αIIbβ3 Clustering. *J. Biol. Chem.* **291**, 11706–11716 (2016).

8. Legate, K. R., Wickstrom, S. A. & Fassler, R. Genetic and cell biological analysis of integrin outside-in signaling. *Genes Dev.* **23**, 397–418 (2009).

9. Huang, J. *et al.* Platelet integrin αIIbβ3: signal transduction, regulation, and its therapeutic targeting. *J. Hematol. Oncol.* **12**, 26 (2019).

10. Wagner, C. *et al.* Analysis of GPIIb/IIIa receptor number by quantification of 7E3 binding to human platelets. *Blood* **88**, 907–914 (1996).

11. Coller, B. S. & Shattil, S. J. The GPIIb/IIIa (integrin αIIbβ3) odyssey: a technology-driven saga of a receptor with twists, turns, and even a bend. *Blood* **112**, 3011–3025 (2008).

12. Oheim, M. & Li, D. Quantitative Colocalisation Imaging: Concepts, Measurements, and Pitfalls. in *Imaging Cellular and Molecular Biological Functions* (eds. Shorte, S. L. & Frischknecht, F.) 117–155 (Springer Berlin Heidelberg, 2007). doi:10.1007/978-3-540-71331-9_5.

13. Pike, J. A., Styles, I. B., Rappoport, J. Z. & Heath, J. K. Quantifying receptor trafficking and colocalization with confocal microscopy. *Methods* **115**, 42–54 (2017).

14. Schulze, H. & Stegner, D. Imaging platelet biogenesis in vivo. *Res. Pract. Thromb. Haemost.* **2**, 461–468 (2018).

15. Clark, J. C. *et al.* Adenosine and Forskolin Inhibit Platelet Aggregation by Collagen but not the Proximal Signalling Events. *Thromb. Haemost.* **119**, 1124–1137 (2019).

409 16. Vangindertael, J. *et al.* An introduction to optical super-resolution microscopy for
410   the adventurous biologist. *Methods Appl. Fluoresc.* **6**, 022003 (2018).

411 17. Levet, F. *et al.* A tessellation-based colocalization analysis approach for single-
412   molecule localization microscopy. *Nat. Commun.* **10**, 1–12 (2019).

413 18. Chen, F., Tillberg, P. W. & Boyden, E. S. Expansion microscopy. *Science* **347**,
414   543–548 (2015).

415 19. Tillberg, P. W. *et al.* Protein-retention expansion microscopy of cells and tissues
416   labeled using standard fluorescent proteins and antibodies. *Nat. Biotechnol.* **34**,
417   987–992 (2016).

418 20. Truckenbrodt, S., Sommer, C., Rizzoli, S. O. & Danzl, J. G. A practical guide to
419   optimization in X10 expansion microscopy. *Nat. Protoc.* **14**, 832–863 (2019).

420 21. Dunn, K. W., Kamocka, M. M. & McDonald, J. H. A practical guide to evaluating
421   colocalization in biological microscopy. *Am. J. Physiol. Physiol.* **300**, C723–C742
422   (2011).

423 22. Manders, E. M. M., Verbeek, F. J. & Aten, J. A. Measurement of co-localization of
424   objects in dual-colour confocal images. *J. Microsc.* **169**, 375–382 (1993).

425 23. van Eeuwijk, J. M. M. *et al.* The Novel Oral Syk Inhibitor, Bl1002494, Protects
426   Mice From Arterial Thrombosis and Thromboinflammatory Brain Infarction.
427   *Arterioscler. Thromb. Vasc. Biol.* **36**, 1247–1253 (2016).

428 24. Richter, K. N. *et al.* Glyoxal as an alternative fixative to formaldehyde in
429   immunostaining and super-resolution microscopy. *EMBO J.* **37**, 139–159 (2018).

430 25. Nieswandt, B., Bergmeier, W., Rackebrandt, K., Gessner, J. E. & Zirngibl, H.
431   Identification of critical antigen-specific mechanisms in the development of
432   immune thrombocytopenic purpura in mice. *Blood* **96**, 2520–2527 (2000).

433 26. Chozinski, T. J. *et al.* Expansion microscopy with conventional antibodies and
434   fluorescent proteins. *Nat. Methods* **13**, 485–488 (2016).

435 27. Truckenbrodt, S. *et al.* X10 expansion microscopy enables 25-nm resolution on
436   conventional microscopes. *EMBO Rep.* **19**, e45836 (2018).

437 28. Arganda-Carreras, I. *et al.* Consistent and Elastic Registration of Histological
438   Sections Using Vector-Spline Regularization. in *Computer Vision Approaches to
439   Medical Image Analysis* 85–95 (2006). doi:10.1007/11889762_8.

440 29. Heil, H. S. *et al.* Sharpening emitter localization in front of a tuned mirror. *Light
441   Sci. Appl.* **7**, 99 (2018).

442 30. Brunstein, M. & Oheim, M. Dependence of descriptors of co-localization on
443   microscope spatiotemporal resolution and the choice of regions of interest.
444   *Microsc. Res. Tech.* **80**, 220–230 (2017).

445 31. Poulter, N. S. *et al.* Clustering of glycoprotein VI (GPVI) dimers upon adhesion to
446   collagen as a mechanism to regulate GPVI signaling in platelets. *J. Thromb.
447   Haemost.* **15**, 549–564 (2017).

448 32. Pallini, C. *et al.* Immobilized collagen prevents shedding and induces sustained
449   GPVI clustering and signaling in platelets. *Platelets* **32**, 59–73 (2021).

450 33. Gaertner, F. *et al.* Migrating Platelets Are Mechano-scavengers that Collect and
451   Bundle Bacteria. *Cell* **171**, 1368-1382.e23 (2017).

452   34.   Nicolai, L. *et al.* Vascular surveillance by haptotactic blood platelets in
453   inflammation and infection. *Nat. Commun.* **11**, 5778 (2020).

454   35.   Ku, T. *et al.* Multiplexed and scalable super-resolution imaging of three-
455   dimensional protein localization in size-adjustable tissues. *Nat. Biotechnol.* **34**,
456   973–981 (2016).

457   36.   Gambarotto, D. *et al.* Imaging cellular ultrastructures using expansion microscopy
458   (U-ExM). *Nat. Methods* **16**, 71–74 (2019).

459   37.   Zwettler, F. U. *et al.* Molecular resolution imaging by post-labeling expansion
460   single-molecule localization microscopy (Ex-SMLM). *Nat. Commun.* **11**, 3388
461   (2020).

462   38.   Rayes, J., Watson, S. P. & Nieswandt, B. Functional significance of the platelet
463   immune receptors GPVI and CLEC-2. *J. Clin. Invest.* **129**, 12–23 (2019).

464   39.   Senis, Y. A., Mazharian, A. & Mori, J. Src family kinases: at the forefront of
465   platelet activation. *Blood* **124**, 2013–2024 (2014).

466   40.   Lee, F. A. *et al.* Lipid rafts facilitate the interaction of PECAM-1 with the
467   glycoprotein VI-FcR γ-chain complex in human platelets. *J. Biol. Chem.* **281**,
468   39330–39338 (2006).

469   41.   Battinelli, E. M. *et al.* Megakaryocytes package contents into separate a-granules
470   that are differentially distributed in platelets. *Blood Adv.* **3**, 3092–3098 (2019).

471   42.   Yadav, S. & Storrie, B. The cellular basis of platelet secretion: Emerging
472   structure/function relationships. *Platelets* **28**, 108–118 (2017).

473   43.   Gao, M. *et al.* Expansion Stimulated Emission Depletion Microscopy (ExSTED).
474   *ACS Nano* **12**, 4178–4185 (2018).

475   44.   Halpern, A. R., Alas, G. C. M., Chozinski, T. J., Paredez, A. R. & Vaughan, J. C.
476   Hybrid Structured Illumination Expansion Microscopy Reveals Microbial
477   Cytoskeleton Organization. *ACS Nano* **11**, 12677–12686 (2017).

478   45.   Mahecic, D., Testa, I., Griffié, J. & Manley, S. Strategies for increasing the
479   throughput of super-resolution microscopies. *Curr. Opin. Chem. Biol.* **51**, 84–91
480   (2019).
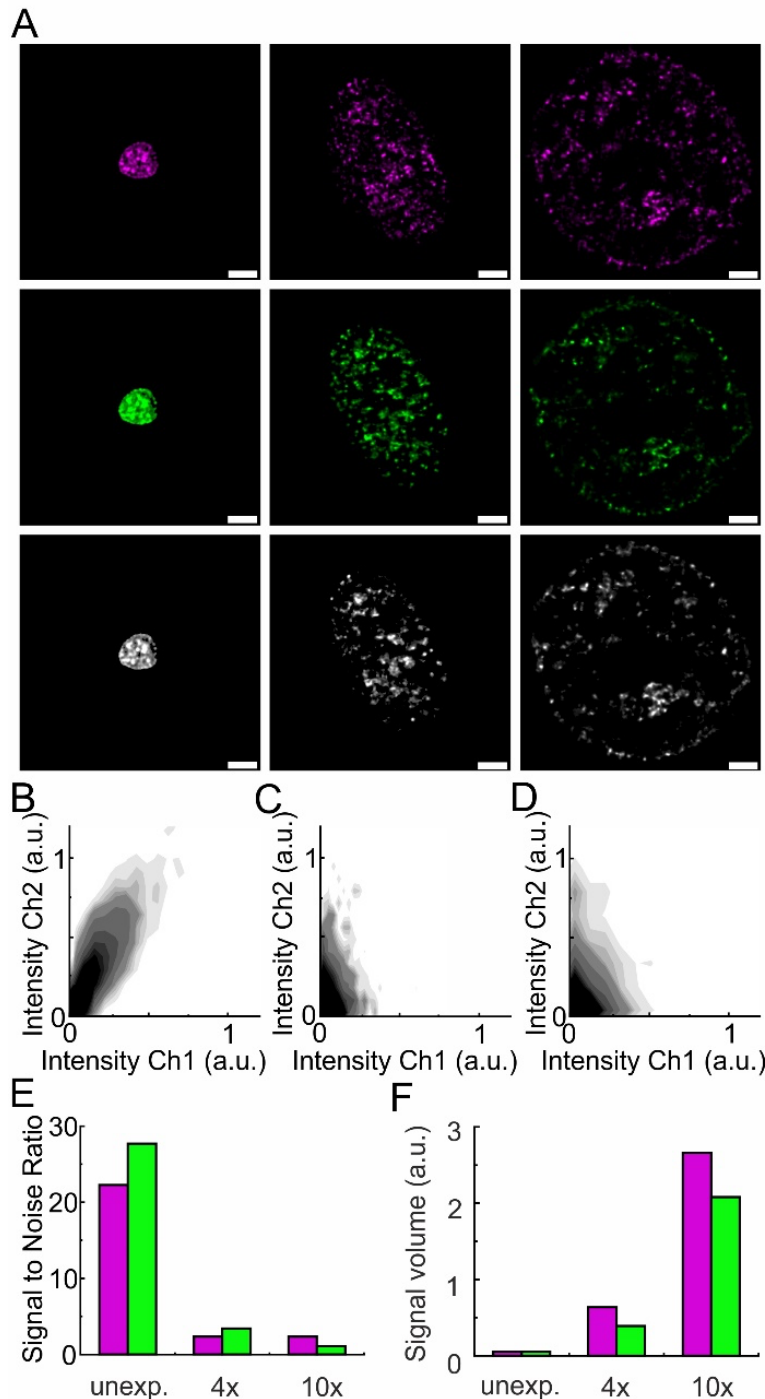
481

482

483   **Figures and captions:**

Figure 1. Colocalization analysis of receptor distributions on expanded platelets.

A, Deconvolved confocal image planes of the GPIIb/IIIa receptor distribution in unexpanded (left panels), 4x expanded (middle panels) and 10x expanded (right panels) resting platelets immunolabeled with the monoclonal antibody MWReg30 (magenta:

Alexa Fluor 594, green: Alexa Fluor 488, white: merged). **B-D,** Density plots of the signal intensities in channel 1 (Ch1, MWReg30-Alexa Fluor 594) and channel 2 (Ch2, MWReg30-Alexa Fluor 488) in logarithmic scale **(B)** unexpanded, **(C)** 4x expanded and **(D)** 10x expanded. **(E-F)** Signal to noise ratio **(E)** and signal volume **(F)** of the respective color channels derived from raw images in **(A)**. Scale bars 3 µm.

484
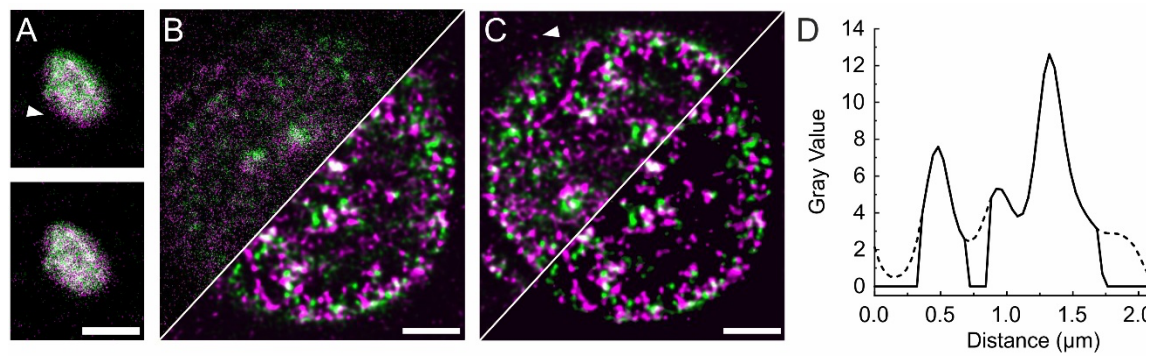
Figure 2. Image preprocessing.

Prior to the colocalization analysis confocal z-stacks of GPIIb/IIIa receptor distributions (MWReg30; green: Alexa Fluor 488, magenta: Alexa Fluor 594) are processed by **(A)** a chromatic shift correction: raw unexpanded platelet, **(B)** image deconvolution: raw (left) and deconvolved (right) image of 4x expanded platelet, **(C)** masking the surface: deconvolved (left) and masked surface (right) of 4x expanded platelet. **(D)** Line plots of signal intensity before (dashed line) and after creating a masked surface (solid line) derived from images in **(C)**. Scale bars 3µm.

485
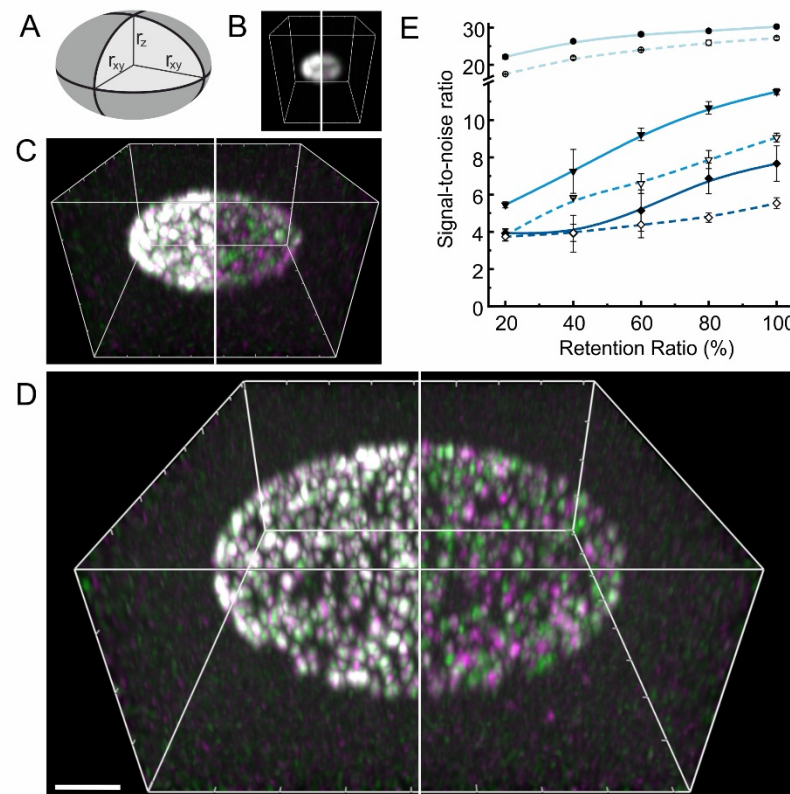
Figure 3. Simulated platelet receptor distributions.

A, Randomly distributed single GPIIb/IIIa receptors or receptor clusters positions were placed on a spheroid surface reflecting typical mouse platelet dimensions (r_{xy} = 1.5 µm and r_z = 0.5 µm). **B-D,** Based on the simulated receptor distributions and the antibody and marker combination (Case I: left, Case II: right) realistic 3D fluorescence images were created including the generation of background signal and noise for **B** unexpanded, **C** 4x expanded (brightness increased 2x) and **D** 10x expanded platelets (brightness increased 10x). In the images presented here the marker retention ratio is 100%. **E,** Signal-to-noise ratio of simulated 3D images in Case I (solid lines, filled symbols) and Case II (dashed lines, open symbols) of unexpanded (light blue), 4x expanded (medium blue) and 10x expanded platelets for a marker retention ratio ranging from 20% to 100%. Scale bar B-D 4 µm
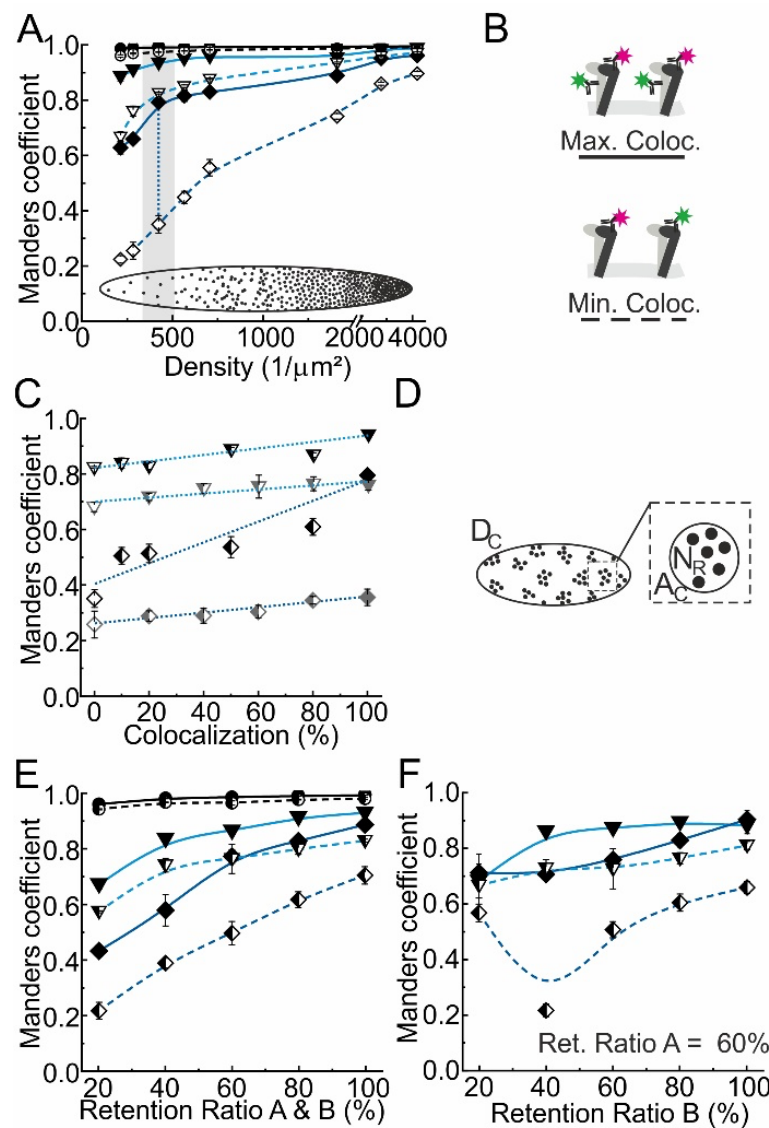
486

Figure 4. Investigating the influence of receptor densities and label retention ratios of the accuracy and resolution of colocalization analysis with ExM based on simulated receptor distributions.

A, Density dependence of the Manders' coefficients for the maximum (solid lines & filled symbols) and minimum (dashed lines & open symbols) colocalization cases illustrated in (B); non-interacting receptor distributions on unexpanded (black), 4x expanded (light blue) and 10x expanded platelets (dark blue) with corresponding SD (error bars). The lines show the trend with a B-spline, the gray shaded area highlights the expected range of the average density of GPIIb/IIIa receptors and the dotted line indicates the dynamic range of the Manders' coefficient. **B,** Cartoon of the maximum and minimum colocalization test case. **C,** Manders' coefficients with

corresponding SD (error bars) of simulated receptor distributions with different degrees of colocalization on 4x (triangles) and 10x (diamonds) expanded platelets for a label retention ratio of 100% (black symbols) and 50 % (gray symbols) with a linear fit (dotted lines) at the receptor density expected for GPIIb/IIIa (dotted line in in A). **D,** Cartoon of a clustered receptor distribution indicating the cluster density D_C, cluster area A_C and the number of receptors per cluster N_R (for GPIIb/IIIa: D_C=70 µm^{-1}, A_C=300 nm and N_R=7, see supplemental Figure III). **E,F** Manders' coefficients with corresponding SD (error bars) in simulated receptor cluster distributions for the maximum (solid lines, filled symbols) and minimum (dashed lines, half-filled symbols) colocalization test cases in the case of **(E)** equal and **(F)** asymmetric scenarios of label retention, unexpanded (black), 4x expanded (light blue) and 10x expanded platelets (dark blue).
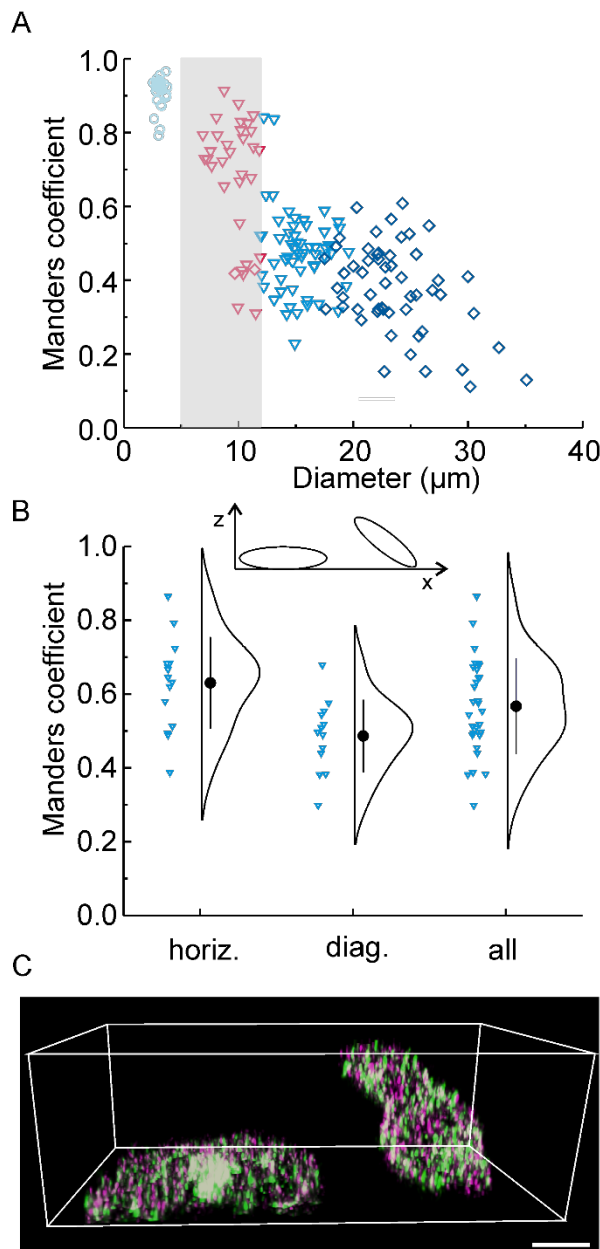
487

488

Figure 5. Manders' colocalization coefficient dependence on expansion factor and orientation.

A, Manders' colocalization coefficient vs. diameter of unexpanded (circles), 4x expanded (triangles) and 10x expanded (diamonds) resting platelets labeled with anti-GPIIb/IIIa antibodies (MWReg30) carrying Alexa Fluor 488 and anti-GPIX antibodies (p0p6) carrying Alexa Fluor 594 (Case III). Expanded platelets with a diameter below 12 µm were excluded from further analysis (marked in red) (**B-C**) **B,** Distributions of the

Manders' colocalization coefficients of 4x expanded resting platelets labeled with an anti-GPIIb/IIIa antibody (MWReg30) carrying either Alexa Fluor 488 (green in C) or Alexa Fluor 594 (magenta in C, Case II) selected for horizontal (horiz.) or diagonal (diag.) orientation and without any selection (all).**C,** Two example platelets from the data in B exhibiting horizontal (left) and diagonal (right) orientation. Scale bar 4 µm
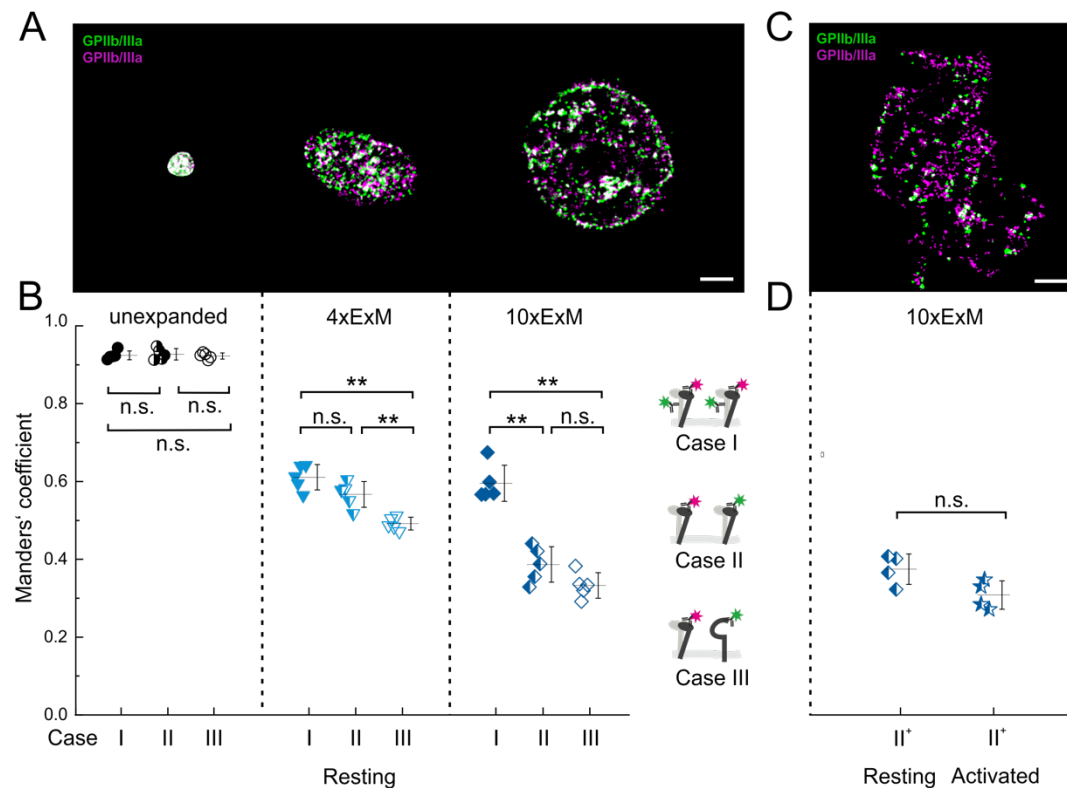
489

Figure 6. Performance of ExM based colocalization analysis.

A, Deconvolved confocal image slices of GPIIb/IIIa receptors on unexpanded (left), 4x expanded (middle) and 10x expanded (right) resting platelets,all directly labeled with fluorescent antibodies (Alexa Fluor 488 (green) or Alexa Fluor 594 (magenta). **B,** Comparing the distributions of the average Manders' coefficients of groups of six with corresponding SD (error bars) of unexpanded (left, black circles), 4x expanded (middle, light blue triangles) and 10x expanded (right, dark blue diamonds) resting platelets labeled with three different combinations of antibodies (Case I: filled symbols, Case II: half-filled symbols & Case III: open symbols). **C,** Deconvolved confocal image slice of GPIIb/IIIa receptors on a 10x expanded activated platelet, directly labeled with fluorescent antibodies (Alexa Fluor 488 (green) or Alexa Fluor 594 (magenta).**D,** Distributions of the average Manders' coefficients of groups of five with corresponding SD (error bars) of 10x expanded resting (dark blue diamonds) and activated platelets (dark blue stars) with labeling scheme Case II$^+$ (Antibody batch 2 with lower density of labeling, see supplemental Table I). n.s.: $p > 0.05$, *: $p \le 0.05$, **: $p \le 0.01$, (Kruskal-Wallis ANOVA test), scale bars 5 μm.

490